HHS Public Access

Author manuscript

Bioconjug Chem. Author manuscript; available in PMC 2019 August 08.

Published in final edited form as:

Bioconjug Chem. 2018 April 18; 29(4): 1209–1218. doi:10.1021/acs.bioconjchem.8b00004.

Ferritin Nanocages with Biologically Orthogonal Conjugation for Vascular Targeting and Imaging

Makan Khoshnejad[*,†,#], **Colin F. Greineder**[*,†,¶,#], **Katherine W. Pulsipher**[§], **Carlos H. Villa**[†], **Burcin Altun**[‖], **Daniel C. Pan**[†], **Andrew Tsourkas**[‖,¶], **Ivan J. Dmochowski**[§,¶], **Vladimir R. Muzykantov**[*,†,¶]

[†]Department of Pharmacology, The Perelman School of Medicine, University of Pennsylvania, Philadelphia, Pennsylvania 19104, United States

[§]Department of Chemistry, The School of Arts and Sciences, University of Pennsylvania, Philadelphia, Pennsylvania 19104, United States

[‖]Department of Bioengineering, The School of Engineering and Applied Sciences, University of Pennsylvania, Philadelphia, Pennsylvania 19104, United States

[¶]Center for Targeted Therapeutics and Translational Nanomedicine (CT3N), University of Pennsylvania, Philadelphia, Pennsylvania 19104, United States

Abstract

Genetic incorporation of biologically orthogonal functional groups into macromolecules has the potential to yield efficient, controlled, reproducible, site-specific conjugation of affinity ligands, contrast agents, or therapeutic cargoes. Here, we applied this approach to ferritin, a ubiquitous iron-storage protein that self-assembles into multimeric nanocages with remarkable stability, size uniformity (12 nm), and endogenous capacity for loading and transport of a variety of inorganic and organic cargoes. The unnatural amino acid, 4-azidophenylalanine (4-AzF), was incorporated at different sites in the human ferritin light chain (hFTL) to allow site-specific conjugation of alkyne-containing small molecules or affinity ligands to the exterior surface of the nanocage. The optimal positioning of the 4-AzF residue was evaluated by screening a library of variants for the efficiency of copper-free click conjugation. One of the engineered ferritins, hFTL-5X, was found to accommodate ~14 small-molecule fluorophores (AlexaFluor 488) and 3–4 IgG molecules per nanocage. Intravascular injection in mice of radiolabeled hFTL-5X carrying antibody to cell adhesion molecule ICAM-1, but not control IgG, enabled specific targeting to the lung due to high basal expression of ICAM-1 (43.3 ± 6.99 vs 3.48 ± 0.14%ID/g for Ab vs IgG). Treatment of mice with endotoxin known to stimulate inflammatory ICAM-1 overexpression resulted in 2-fold

[*]**Corresponding Authors:** makank@mail.med.upenn.edu., cgreineder@gmail.com., muzykant@mail.med.upenn.edu.
[#]Makan Khoshnejad and Colin F. Greineder contributed equally to this work.

ASSOCIATED CONTENT

Supporting Information

The Supporting Information is available free of charge on the ACS Publications website at DOI: 10.1021/acs.bioconj-chem.8b00004. Generation of FTL-X variant library, Evaluation of FTL-5X variant conjugation efficiency, Native PAGE, TEM, HPLC, and SDS-PAGE analysis of FTL-X variants, SDS-PAGE analysis of FTL-5X, *In vivo* targeting of ^{111}In-labeled targeted FTL-5X to ICAM-1, and Tables for raw data of biodistribution studies (PDF)

Notes

The authors declare no competing financial interest.

enhancement of pulmonary targeting (84.4 ± 12.89 vs 43.3 ± 6.99%ID/g). Likewise, injection of fluorescent, ICAM-targeted hFTL-5X nanocages revealed the effect of endotoxin by enhancement of near-infrared signal, indicating potential utility of this approach for both vascular targeting and imaging.

Graphical Abstract

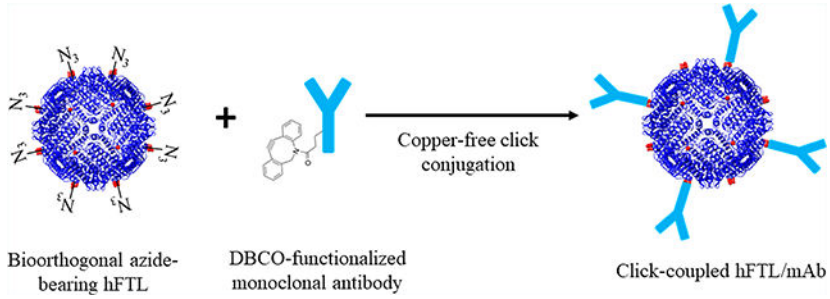

INTRODUCTION

Nature has created a number of molecules with unique architectures and properties suitable for transporting and delivering cargo to specific cells or sites within the body. Among them, the iron-storage protein ferritin is perhaps the strongest candidate for clinical application, given its presence not only within every cell of the human body, but also the extracellular space and circulating plasma.[1,2] Ferritin displays remarkable thermal stability (withstanding temperatures up to 80–100 °C), resistance to extreme variation in pH, small size (12 nm in diameter), monodispersity, and a large central cavity for encapsulation of metals, small molecule drugs, contrast agents, and even other nanoparticles.[3–16] Human ferritin heavy (hFTH) and light (hFTL) chains are also easily expressed in a variety of microbial expression systems, making their production possible at relatively low cost and large scale.[17–19]

While ferritin nanocages are themselves recognized and endocytosed by a number of cell surface receptors,[20,21] their specificity is limited, preventing their use in the vast majority of drug delivery and molecular imaging applications. To achieve targeted ferritin delivery, more selective ligands of cell surface markers, such as antibodies, can be conjugated to ferritin. For example, intravenous injection of apoferritin nanocages conjugated with antibody to intracellular cell adhesion molecule, ICAM-1, provides targeting to the pulmonary vasculature in mice.[22] Antibodies and other affinity ligands can be conjugated to ferritin either using chemical cross-linking to the reactive amino acid side chains or via genetic fusion with recombinant ferritin.[23,24] Chemical conjugation of natural proteins provides very limited, if any control of which amino acid(s) of ferritin are modified, hence it yields heterogeneous molecular species with variable degree of modification (DOM). Recombinant fusion bypasses this challenge and yields homogeneous molecular species, but restricts conjugation of targeting moieties to either N- or C-terminus of the ferritin molecule and requires identification of affinity ligands that will fold properly while not sterically interfering with nanocage self-assembly.[25–27]

An attractive alternative to each of these methods is the incorporation of unnatural amino acids (uAAs)[28–30] into the hFTL or hFTH polypeptide chain. In addition to site-specificity, uAAs allow introduction of a range of functionalized amino acid side chains, including those bearing bioorthogonal reactive groups like azides, alkynes, alkenes, and tetrazines.[31,32] While many approaches have been described, the most commonly utilized system relies on expansion of the genetic code by coexpression of aminoacyl-tRNA synthetase (aaRS) and tRNA pairs from orthogonal species like *P. horikoshii* and *M. jannaschii*.[33] This approach results in suppression of the amber stop codon and enables incorporation of the unnatural amino acid at nearly any site in the protein.[28,32] Among other applications, the introduction of unnatural amino acids has been used to make potent antibody-drug conjugates[34] and to functionalize the surface of certain bacteriophage-derived virus-like particles (VLPs).[35]

Here, we extend the use of uAA to ferritin, using the existing hFTL crystal structure to identify surface-displayed amino acids for replacement with 4-azidophenylalanine (4-AzF). Multiple hFTL mutants, each with a different site of 4-AzF incorporation, are screened for two important parameters: 1, nanocage assembly and structure; and 2, accessibility of the azide side chain for conjugation of a dibenzylcyclooctyne (DBCO)-modified fluorophore. The optimal clone is then modified with a DBCO-functionalized monoclonal antibody specific for murine ICAM-1 to enable targeting of this cell adhesion molecule *in vitro* and *in vivo*. Finally, the resulting conjugate is used for near-infrared imaging of endotoxin-induced lung injury, providing proof of principle for use of genetically engineered hFTL nanocages as agents for molecular imaging of pulmonary vascular inflammation.

RESULTS

Construction and Characterization of hFTL-X Variants and Conjugates.

Figure 1 shows the overall schema for cloning, transformation, production, and purification of the genetically engineered human ferritin light chain (hFTL) mutants. PCR mutagenesis was used to incorporate an amber stop codon (TAG) at various positions in the human FTL cDNA, corresponding to residues 2, 5, 9, 79, 83, 105, 112, and 155. Figure S1A shows the results of an analysis of the solvent accessible surface area (SASA) of the side chain of each of these amino acids, calculated using the GETAREA algorithm[36] and a 2.5 Å resolution hFTL crystal structure.[37] Figure S1B shows the approximate position of each of the selected amino acids on ribbon diagrams of the hFTL monomer and assembled 24-mer.

In general, the candidate residues were chosen based on three parameters: 1, exposure to the external surface of the nanocage (based on the location of the side chain in the published crystal structure); 2, solvent accessible surface area; and 3, similarity of the native amino acid structure to that of azidophenylalanine (with the idea that this would minimize the potential impact of uAA incorporation on the structure of the assembled nanocage). One of the clones, FTL-155X, was chosen despite relatively low side chain solvent accessible surface area (SASA), due to previous reports of successful insertion of peptide affinity ligands between the D and E helices of hFTL. Likewise, the ninth residue, which had a predicted side chain SASA of 0, was chosen as a comparison to determine potential correlation between predicted solvent exposure and accessibility of the azide side chain to its bioorthogonal partner.

Following synthesis and purification, each genetically engineered hFTL-X mutant was evaluated with a combination of native and/or denaturing SDS-PAGE, TEM, and size exclusion HPLC to confirm proper assembly into nanocages (Figures S3–S6). With the SDS-PAGE analysis, the monomeric human ferritin light chains can be observed at their predicted molecular weight of around 19 kDa. In order to determine the optimal conjugation efficiency of FTL-X variants, DBCO-alexafluor488 was used as a model conjugation moiety. The conjugation reactions were carried out at room temperature overnight, followed by quantitative TLC. The conjugations efficiencies (Figure S2) were as follows: (1) hFTLX-2 (30%), (2) hFTLX-5 (57%), (3) hFTLX-9 (10%), (4) hFTLX-79 (14%), (5) hFTLX-83 (16%), (6) hFTLX-105 (18%), (7) hFTLX-112 (14%), and (8) hFTLX-155 (18%). No clear correlation was seen between the SASA values and the conjugation efficiency of the various mutants. One potential reason for variability could be various degrees of aggregation of the purified FTL variants. Additional FPLC purification steps could lead to more homogeneous population of variants and possibly better conjugation efficiencies. The two unnatural amino acid incorporation sites with the highest efficiency (hFTLX-2 and hFTLX-5) were positioned at the very N-terminal region of hFTL, where the N-terminus of human ferritin subunit is exposed to the exterior. Interestingly the unnatural amino acid sites toward the most C-terminus region did not perform well in conjugation studies. Relative to the fully assembled ferritin crystal structure, the best performing engineered ferritins are positioned at very N-terminal extension region exposed on the outside surface of the ferritin shell. Out of the eight different positions tested throughout hFTL, the fifth amino acid position was found to be, by far, the optimal position for conjugation of a small molecule fluorophore, showing 57% efficient click conjugation to DBCO-Alexafluor 488. Based on these results, hFTLX-5 was chosen as the primary FTL for conjugation purposes with larger moieties such as antibodies.

Characterization of hFTL-5X and Antibody Conjugates.

SDS-PAGE analysis of the synthesis and purification of hFTL-5X is shown in Figure S7. In particular, a band at the expected size of an hFTL monomer (~19 kDa) is seen in the lysate of bacteria grown in the presence of AzF but not in its absence, indicating successful suppression of the amber stop codon. Based on both HPLC (Figure S5) and SDS-PAGE (Figure S7), the purity of hFTL-5X was >95% following heat precipitation of bacterial lysate and purification on FPLC. hFTL-5X was conjugated with fluorescently labeled mouse ICAM-1 monoclonal antibody (i.e., anti-ICAM) at different molar ratios of 1 to 2 and 1 to 10 and analyzed by Western blot, fluorescence scanning, and SDS-PAGE (Figure 2a–c). At both ratios and particularly at the higher 1 to 10 molar ratio, conjugate bands can be observed at above 180 kDa molecular weight marker, indicating full-length antibody conjugated to single or multiple hFTL monomers.

Transmission electron microscope (TEM) imaging of hFTL-5X and hFTL-5X/antibody conjugates shows small uniform spherical structures (Figure 2e,f). TEM images correspond with DLS size analysis, showing hFTL-5X nanocages averaging 10.2 ± 0.2 nm with polydispersity index 0.25 ± 0.01. The HPLC-purified hFTL-5X/antibody conjugates averaged 27.9 ± 2.7 nm in diameter with polydispersity index of 0.24 ± 0.05. hFTL-5X

exhibits uniform small sized structure capable of click-coupled antibody conjugation, suitable as carriers for targeted drug delivery and imaging.

Quantification of Number of Antibody Molecules Conjugated to hFTL-5X.

Radioisotope HPLC analysis was performed to quantify number of antibodies conjugated to DBCO-modified anti-ICAM. Antibody was 125I-labeled followed by click coupling to FTL-5X overnight at rt. hFTL-5X HPLC fractions of hFTL-5X/antibody conjugates were collected every minute and measured with a gamma counter. As shown in Figure 3, calculation of areas under the curve (AUC) for conjugate vs free antibody indicates attachment of 1.26, 2.81, and 3.46 antibodies per hFTL-5X nanocarrier at for molar ratios of 1:2, 1:5, and 1:10, respectively. This suggests that a nanocarrier decorated with varying numbers of affinity ligands can be synthesized by altering the stoichiometry of the conjugation reaction. For subsequent experiments involving antibody-targeted hFTL-5X, a stoichiometry of 1 to 10 was chosen.

In vitro Binding of Targeted hFTL-5X Nanocarriers.

Binding of targeted hFTL-5X/anti-ICAM conjugates was evaluated using wild type REN cell line of a human mesothelioma cells that does not express mouse ICAM-1, vs REN-ICAM cells which stably overexpress mouse ICAM-1. hFTL-5X was iodine-125 labeled, followed by click conjugation to anti-ICAM. As demonstrated in Figure 3e, selective binding can be observed to REN-ICAM cells, compared to essentially background level in REN wild type cells. These results demonstrate selective binding in an artificial model to specific endothelial cell adhesion molecule.

Targeted Delivery of ^{125}I- or ^{111}In-Labeled hFTL-5X Nanocarriers to Pulmonary Endothelium *In vivo*.

To investigate biodistribution of targeted hFTL-5X nanocarriers in mice, two different radiolabeling strategies were utilized (Figures 4 and S8). First, iodine-125 labeling of hFTL-5X was performed followed by antibody click-coupling. Lipopolysaccharide (LPS) administration has been reported to stimulate endothelial cells and upregulate expression of proinflammatory cytokines and cell adhesion markers (CAMs) such as ICAM-1. Here we investigated the effect of LPS-induced endotoxemia on enhancing pulmonary endothelial delivery.

Pulmonary uptake with targeted hFTL-5X/anti-ICAM was enhanced 2-fold upon intravenous administration of LPS, increasing from 43.3 ± 7.0%ID/g in naive to 84.4 ± 12.9%ID/g in LPS-treated mice. The lung localization ratio was similarly enhanced from 14.7 ± 2.8 in naive mice to 23.9 ± 7.0 in LPS administered mice. No selective pulmonary uptake or enhancement with LPS was observed with hFTL-5X/IgG2b control mice.

A second radioisotope indium-111 was used for evaluating biodistribution of targeted hFTL-5X. For loading 111In radioisotopes in FTL, we chemically conjugated using DOTA-NHS ester onto hFTL-5X surface, followed by click coupling to anti-ICAM. Loading of indium-111 onto DOTA chelator-conjugated hFTL-5X/anti-ICAM was carried out at ratio of 1:1 ratio 1 μCi/μg, 1 h at 37 °C. The ^{111}In-labeled conjugates had a radiochemical purity of

~70%. Similar to iodine-125 biodistribution study, there was a significant increase in pulmonary uptake upon LPS administration. Pulmonary uptake increased from 32.4 ± 2.2%ID/g in naive to 50.5 ± 5.7 in LPS-treated mice. The lung localization ratio increased from 7.3 ± 0.6 in naive to 10.3 ± 0.6 in LPS administered mice. Both ^{125}I- or ^{111}In-labeled targeted hFTL-5X nanocarriers demonstrated selective pulmonary uptake and enhancement of uptake in LPS-challenged mice. This elevation in pulmonary uptake in pathologic conditions can be very valuable in imaging pulmonary inflammation.

Imaging Inflammation-Associated ICAM Up-Regulation in Endotoxin-Challenged Animals.

Next, we have detected inflammation induced by LPS in animals using nonradioactive near-infrared imaging modality. Near-infrared fluorescence probe Alexafluor 750 was chemically conjugated to hFTL-5X following by click coupling to anti-ICAM. Mice were treated with LPS as in the experiment described above, injected intravenously with NIR-labeled conjugates and euthanized 30 min later. Major organs were harvested for imaging with PerkinElmer IVIS Spectrum *In vivo* Imaging System. As shown in Figures 5 and S9, substantial enhancement in pulmonary uptake can be observed in LPS-treated mice. The radiant efficiency (p/s/cm^2/sr)/(μW/cm^2) of lung tissue for mice administered hFTL-5X/anti-ICAM nanocarriers, increased from 4.84×10^8 in naive mice to 6.91×10^8 in LPS-treated mice, corresponding with radiolabeled FTL-5X biodistribution studies (Tables S1–2).

DISCUSSION

Many therapeutic delivery systems have been developed with unique properties that make them valuable for different applications in medicine. These include naturally occurring and engineered recombinant protein-based systems,[38–43] synthetic nanoparticles,[44–53] and physical delivery systems.[54–56] Targeted drug delivery systems have been developed to reduce side-effects and maximize efficiency. Active targeting strategies have been developed via conjugation of various targeting ligands to deliver therapeutics to the desired pathological tissue. Three major issues with conventional conjugation strategies are the lack of control over the number of cross-linkers attached, the orientation of the conjugated protein, and aggregation. Site-specific conjugation has been used to develop more homogeneous, reproducible, and potent biotherapeutics. Nanomedicine can benefit greatly from production of a biocompatible, site-specific conjugatable, homogeneous, and scalable delivery system that can be used for both drug delivery and imaging. Here we genetically modified the human ferritin light chain to incorporate the unnatural amino acid azidophenylalanine for development of a fully assembled bionanoparticle displaying 24 azide moieties for bioconjugation to targeting moieties or cargoes. The amber suppressor nonsense codon (TAG) was incorporated in various positions throughout the FTL to determine the ideal sites for click-coupled conjugation.

Strain-promoted azide–alkyne cycloaddition (SPAAC) click chemistry also called copper-free click chemistry is a very efficient bioconjugation strategy between an azide and cyclooctyne moiety that is compatible in a broad range of reaction conditions.[57] One novel strategy that has been used to incorporate clickable functional moieties in proteins has been the utilization of orthogonal systems of unnatural amino acids and orthogonal amino-acyl

tRNA synthetase/tRNApairs. The unnatural amino acids can be used to incorporate a range of clickable and other functional groups such as azides, alkynes, alkenes, and tetrazines.[28–32] Selective incorporation of amber stop codon into the gene of interest followed by cotransformation in *E. coli* host for protein production and administration of the unnatural amino acid to the host, allows for site-specific incorporation of the unnatural amino acid into the protein. This orthogonal uAA incorporation strategy has been developed in both prokaryotic and eukaryotic systems.[58–60] Prokaryotic protein expression systems such as with *E. coli* have become a very cost-effective and efficient strategy for industrial-scale production of therapeutic proteins. Some examples of FDA-approved proteins in *E. coli* include Humulin N (insulin human recombinant), Protropin (human growth hormone), Filgrastim (human granulocyte colony stimulating factor), Palifermin (human keratinocyte growth factor), and Pegloticase (mammalian uricase).[61,62] Both prokaryotic and eukaryotic expression systems could be used for large-scale production of azide-bearing FTL for various applications.

In the present study, we developed genetically engineered human ferritin light chain incorporating biorthogonal azide-bearing unnatural amino acids for site-specific conjugation of antibodies as a targeted drug delivery system. We utilized the most optimal clickable FTL variant, hFTL-5X for evaluation in pulmonary targeted delivery and imaging. For conjugation to larger macromolecules such as DBCO-antibodies, we determined an optimal molar ratio of 1 to 10 hFTL-5X to antibody, which yielded 3.46 antibodies per FTL-5X 24mer. This corresponded with our previous work on random chemical conjugation of antibodies to horse spleen apoferritin, which was roughly 3.9 antibodies per ferritin.[22] To further evaluate the potential of the targeted hFTL-5X nanocarriers, biodistribution studies were performed in normal and LPS treated mice to determine selective pulmonary targeting, as well as differences in targeting between natural and inflamed pathological vascular conditions. Two different radiolabeling strategies (iodine-125 and indium-111) as well as a near-infrared fluorescent probe labeling of hFTL-5X were used. Selective pulmonary uptake was demonstrated with ^{125}I-labeled FTL-5X/anti-ICAM along with a substantial 2-fold enhancement in targeting in inflamed conditions, increasing from 43.3 ± 7.0%ID/g in naive to 84.4 ± 12.9%ID/g in LPS-treated mice.

Potential applications of the advanced approach described in this manuscript for conjugation targeting moieties with carriers and cargoes include optimization of delivery of therapeutic, imaging and other pharmacological agents in the body, either in animal studies or, in the more distant future, perhaps in the clinical practice. Note that utility in animal studies is not limited to the preclinical testing of medical interventions, and includes modeling of human pathology and veterinary use. Each of these animal and human applications has a unique set of specifications, such as degree of specificity, selectivity, pharmacokinetic, biodistribution, delivered dose, onset timing, duration, localization, and amplitude of the effects. One question relevant to these specifications is whether 2-fold enhancement of targeting such as reported here can provide a tangible improvement in any of these applications. Arguably, 2-fold reduction of systemic dose might alleviate off-target unintended effects in drug delivery, whereas 2-fold increase in target/nontarget ratio of localization of imaging probes may significantly enhance the resolution and selectivity of imaging. In particular, 2-fold enhancement of selectivity of imaging ICAM-1 upregulation in animal models of acute

pulmonary inflammation afforded better imaging.[63–65] However, the results presented in this paper pertain more to the proof of principle for site-specific conjugation illustrated by a specific example of targeting to endothelial adhesion molecules, not an appraisal of particular practical utility of the approach. Targeted biocompatible nanocarriers for imaging pulmonary inflammation or treatment can be very valuable in pulmonary critical care medicine. These results demonstrate the targeting potential of hFTL-5X for bioimaging and therapeutic applications. Moreover, production of a fully assembled biocompatible nanocarrier capable of site-specific conjugation to targeting moieties and cargoes could be very valuable in the translation of nanomedicine for clinical applications.

CONCLUSION

In summary, we genetically engineered human FTL to create a novel, clickable nanocage ready-made for site-specific conjugation of targeting ligands and/or cargo. Through site-selective modification of FTL with unnatural amino acids, we determined the fifth amino acid position to be the optimal site for click conjugation. The engineered FTL nanocages displayed 24 azide groups for bioconjugation to antibodies or cargo molecules. Through radioHPLC quantification, around 3.46 antibodies were found to be conjugated to FTL-5X 24mer protein. Biodistribution studies investigating the ability to target inflamed pulmonary vasculature were performed using three different tracing probes, iodine-125, indium-111, and Alexa-fluor750 NIR fluorophore. These biodistribution studies using the different probes all showed selective pulmonary uptake and substantial enhancement upon LPS administration, demonstrating their potential for imaging or treatment of inflammatory pulmonary conditions. These engineered customizable biological nanocarriers can be easily tailored to display various targeting moieties in a multivalent fashion enabling targeted delivery. With their remarkable stability, relatively small, uniform nature, and capacity for site-specific modification, these engineered nanocarriers have tremendous potential in nanomedicine, particularly in pulmonary medicine, where there is a lack of efficiently targeted drug delivery vehicles.

METHODS

Ethics Statement.

Animal studies were carried out in accordance with the Guide for the Care and Use of Laboratory Animals as adopted by the NIH, under protocols 805837 and 805708 approved by University of Pennsylvania IACUC.

Cell Lines, Antibodies, and Other Reagents.

REN cells (human mesothelioma) were grown to confluence in RPMI 1640 medium with 10% fetal bovine serum supplemented with 2 mM L-glutamine, 100 U/mL penicillin, and 100 μg/mL streptomycin (Life Technologies, Carlsbad, CA). T7 Express Crystal Competent *E. coli* (C3022I) was purchased from New England Biolabs (Ipswich, MA). 4-Azido-L-phenylalanine (sc-289923A) was purchased from Santa Cruz Biotechnology Inc. (Dallas, TX). EDTA-Free SIGMAFAST Protease Inhibitor Cocktail Tablets (S8830), dibenzocyclooctyne-*N*-hydroxysuccinimidyl ester (761524) were purchased from Sigma-

Aldrich (St. Louis, MO). Click-IT Alexa Fluor 488 DBCO (C10405) and Alexafluor750 Succinimidyl Ester (A20011) were purchased from ThermoFisher Scientific (Waltham, MA). Iodogen was purchased from Pierce Biotechnology (Rockford, IL). Radioactive isotope 125I was purchased from PerkinElmer (Wellesley, MA). ^{111}InCl3 was purchased from Nuclear Diagnostic Products (Cherry Hill, NJ). Mouse IgG2B Isotype Control was from R&D Systems, Inc. (Minneapolis, MN). Antimouse-ICAM-1 mAb (clone YN1/1.7.4) was produced by the hybridoma technology[66–69] and purified using protein G Sepharose from GE Healthcare Biosciences (Pittsburgh, PA).

Construction of hFTL-X Variants.

The plasmid pEVOL-pAzF, encoding the azidophenylalanine tRNA/amino-acyl tRNA synthetase (aaRS) pair, was obtained from Addgene (#31186). A full-length cDNA for hFTL (SC120074) was purchased from Origene (Rockville, MD) and cloned into the bacterial expression vector, pRSET A (Thermo Fisher Scientific, Philadelphia, PA). PCR was used to generate 8 mutant cDNAs with the amber stop codon at sites corresponding to amino acid positions 2, 5, 9, 79, 83, 105, 112, or 155 in the hFTL gene product. pRSET plasmids containing the mutant hFTL (referred to as hFTL-2X, 5X, 9X, 79X, 83X, 105X, 112X, and 155X) were cotransformed with pEVOL-pAzF, a plasmid encoding the 4-AzF aminoacyl-tRNA synthetase (aaRS) and tRNA pairs, and bacteria were selected with ampicillin (100 μg/mL) and chloramphenicol (25 μg/ mL).

Production of hFTL-X Variants in *E. coli*.

To produce hFTL-X mutant protein, starter cultures were inoculated from single colonies of cotransformed, antibiotic selected bacteria. These growths were transferred into 1 L of antibiotic-containing LB media and grown to an OD600 of 0.8 prior to induction with 1 mM isopropyl-β-thiogalactopyranoside (IPTG) and addition of 1 mM 4-azido-L-phenylalanine. After an additional 4 h, bacterial growths were harvested by centrifuging at 2400g, 4 °C, for 15 min. Recombinant hFTL mutants were purified from bacterial cells via a method adapted from Luzzago et al.[70] Briefly, cell pellets were resuspended in 40 mL PBS with SIGMAFAST Protease Inhibitor, prior to 6 rounds of probe sonication (QSonica; 30% Amplitude) for 2 min and centrifugation at 3220g, 4 °C, for 20 min. Supernatants were heat precipitated for 10 min at 75 °C, followed by centrifugation at 12397g, 4 °C, for 90 min and filtration with a 0.22 μm filter. Filtered samples were purified by FPLC, using a HiLoad 16/600 Superdex200 prep grade column at a flow rate of 1 mL/min with PBS buffer.

Coupling of AlexaFluor488-DBCO to hFTL-X Nanocages.

To determine the conjugation efficiencies of hFTL-X variants, DBCO-Alexafluor488 was selected as a model conjugation moiety. hFTL-X variants (1 μM final concentration) were incubated with DBCO-Alexafluor488 at molar ratio of 1 to 24 (hFTL-X:DBCO-Alexafluor488). The reactions were carried out overnight at rt. Quantitative thin layer chromatography (TLC) was performed using alumina-backed silica gel with mobile phase of 75% methanol and 25% ammonium acetate to determine the amount of conjugated and free fluorophore.

Preparation of ICAM-1 Targeted hFTL-5X Nanocages.

Prior to conjugation to hFTL-5X nanocages, ICAM-1 specific monoclonal antibody (mAb) was modified with dibenzocyclooctyne-*N*-hydroxysuccinimidyl ester (DBCO-NHS) at a 1:5 molar ratio (mAb:DBCO-NHS) for 1 h at rt. Unreacted NHS ester was removed by G-25 Sephadex Quick Spin Protein Columns (Roche Applied Science, Indianapolis, IN). DBCO-modified mAb was conjugated to FTL-5X (3 μM final concentration) overnight at rt. Reaction mixtures were analyzed to determine conjugation efficiency using size-exclusion high-performance liquid chromatography (SEC-HPLC) with a BioSep SEC-s3000 column (Phenomenex, Torrance, CA) and an isocratic method with 100% PBS pH 7.4. SEC-HPLC was also used to purify conjugates away from free antibody and to analyze purified conjugates. Purified conjugates were also analyzed by SDS-PAGE (4–15% gradient gel) and Western blot.

Characterization of Targeted hFTL Nanocages.

The size of unconjugated and antibody-conjugated hFTL-5X nanocages was measured using a Malvern Zetasizer Nano ZS (Malvern Instruments, Worcestershire, UK). Size measurements were carried out in PBS buffer at 25 °C with a noninvasive back scatter system (NIBS) with scattering angle of 173°. hFTL-X nanocages were also analyzed with JOEL1010 transmission electron microscope (TEM), as previously described.[22]

hFTL-5X Radiolabeling.

hFTL-5X was labeled with radioactive ^{125}I isotope purchased from PerkinElmer (Wellesley, MA). The reaction was performed for 15 min at rt using Pierce Iodination Beads. Free 125I was removed by G-25 Sephadex Quick Spin Protein Columns (Roche Applied Science). For Indium-111 radiolabeling of hFTL-5X, $^{111}InCl_3$ was purchased from Nuclear Diagnostic Products (Cherry Hill, NJ). hFTL-5X conjugated DOTA-mono-NHS tris (B-270; Macrocyclics, Plano, TX) loaded with indium-111 at 1:1 ratio 1 μCi/μg, 1 h at 37 °C. Purification was carried out using 10-DG desalting column equilibrated with PBS. TLC was performed using alumina-backed silica gel to determine the percent of free ^{125}I or ^{111}In. For ^{125}I studies, mobile phase consisted of 75% methanol and 25% ammonium acetate. For ^{111}In studies, three different mobile phases were used: 0.9% NaCl/10, 20 mM EDTA, or 0.1 M citric acid. TLC plates were analyzed using a Typhoon 9410 Molecular Imager (GE Healthcare Life Sciences, Pittsburgh, PA). The radiochemical purity was the determined as the area of the free radioisotope divided by the area sum of the total.

Binding of Targeted hFTL Nanocarriers.

Binding of radiolabeled, antibody-conjugated hFTL-5X nanocages was measured using confluent monolayers of mouse ICAM-1 expressing REN cells and wild type control cells. After 1 h incubation at 37 °C, cells were washed three times with ice-cold Hank's Balanced Salt Solution (HBSS, Corning Cellgro, Manassas, VA) followed by lysis with 1% Triton X-100, 1 M NaOH. Bound vs unbound radioactivity was measured using Wallac 1470 Wizard gamma counter (Gaithersburg, MD).

Biodistribution of Radiolabeled Targeted Nanocarriers *in vivo*.

Radiolabeled hFTL-5X nanocarriers were administered intravenously via retro-orbital injection into C57BL/6J mice (The Jackson Laboratory, Bar Harbor, ME). Thirty minutes after injection, blood was collected and the organs were harvested. The radioactivity of the samples was measured with Wallac 1470 Wizard gamma counter (Gaithersburg, MD). The measured radioactivity and weight of the samples were used to calculate percent injected dose per gram (%ID/g).

Near Infrared (NIR) Imaging.

For NIR imaging, hFTL-5X was reacted with Alexafluor750 Succinimidyl Ester (AF750-NHS) for 1 h at rt using a molar ratio of 1 to 50 (hFTL-5X:AF750-NHS). Free fluorophore was removed by G-25 Sephadex desalting column (Roche Applied Science). The AF750 fluorophore was conjugated to the surface amine groups of FTL, as compared to the antibodies which were conjugated onto the azides of the engineered FTL. Like radioiodination, hFTL-5X was labeled with fluorophore prior to conjugation of antibody to ensure tracing of nanocages. Fluorophore-labeled, antibody conjugated hFTL-5X was injected intravenously 30 min prior to euthanization and harvest of the major organs. Organs were imaged *ex vivo* using the PerkinElmer IVIS Spectrum Imaging System (PerkinElmer, Waltham, MA).

Statistical Analysis.

Statistical analysis was performed using Student's *t* test with Bonferroni correction. Differences were deemed statistically significant at $p < 0.05$.

Supplementary Material

Refer to Web version on PubMed Central for supplementary material.

ACKNOWLEDGMENTS

This work is supported by NIH Training Grants T32 HL007954, T32 HL774819, T32 HL07915 and National Heart, Lung and Blood Institute (NHLBI) R01 HL125462–01A1and R01 HL128398.

ABBREVIATIONS

4-AzF	4-azidophenylalanine
hFTL	human ferritin light chain
uAAs	unnatural amino acids
aaRS	aminoacyl-tRNA synthetase
DBCO	dibenzylcycloocytyne
SASA	solvent accessible surface area

REFERENCES

1. Wang W, Knovich M, and Coffman L (2010) Serum ferritin: Past, present and future. Biochim. Biophys. Acta, Gen. Subj 1800, 760–769.
2. Knovich MA, Storey JA, Coffman LG, Torti SV, and Torti FM (2009) Ferritin for the clinician. Blood Rev 23, 95–104. [PubMed: 18835072]
3. Zhen Z, Tang W, Todd T, and Xie J (2014) Ferritins as nanoplatforms for imaging and drug delivery. Expert Opin. Drug Delivery 11, 1913–22.
4. Theil EC (1987) Ferritin: structure, gene regulation, and cellular function in animals, plants, and microorganisms. Annu. Rev. Biochem 56, 289–315. [PubMed: 3304136]
5. Li K, et al. (2012) Multifunctional ferritin cage nanostructures for fluorescence and MR imaging of tumor cells. Nanoscale 4, 188. [PubMed: 22080281]
6. Kitagawa T, et al. (2012) RGD-conjugated human ferritin nanoparticles for imaging vascular inflammation and angiogenesis in experimental carotid and aortic disease. Mol. Imaging Biol 14, 315–24. [PubMed: 21638084]
7. Watt RK (2011) The many faces of the octahedral ferritin protein. BioMetals 24, 489–500. [PubMed: 21267633]
8. Arosio P, Adelman T, and Drysdale J (1978) On ferritin heterogeneity. Further evidence for heteropolymers. J. Biol. Chem 131, 210–6.
9. Harrison PM, and Arosio P (1996) The ferritins: molecular properties, iron storage function and cellular regulation. Biochim. Biophys. Acta, Bioenerg 1275, 161–203.
10. Choi S-H, Choi K, Chan Kwon I, and Ahn HJ (2010) The incorporation of GALA peptide into a protein cage for an acid-inducible molecular switch. Biomaterials 31, 5191–8. [PubMed: 20359742]
11. Liang M, et al. (2014) H-ferritin-nanocaged doxorubicin nanoparticles specifically target and kill tumors with a single-dose injection. Proc. Natl. Acad. Sci. U. S. A 111, 14900–14905. [PubMed: 25267615]
12. Wang Z, et al. (2016) Biomineralization-Inspired Synthesis of Copper Sulfide-Ferritin Nanocages as Cancer Theranostics. ACS Nano 10, 3453–3460. [PubMed: 26871955]
13. Pulsipher KW, Honig S, Deng S, and Dmochowski IJ (2017) Controlling gold nanoparticle seeded growth in thermophilic ferritin protein templates. J. Inorg. Biochem 174, 169–176. [PubMed: 28683348]
14. Pulsipher KW, et al. (2017) Thermophilic Ferritin 24mer Assembly and Nanoparticle Encapsulation Modulated by Interdimer Electrostatic Repulsion. Biochemistry 56, 3596–3606. [PubMed: 28682599]
15. Cheung-Lau JC, Liu D, Pulsipher KW, Liu W, and Dmochowski IJ (2014) Engineering a well-ordered, functional protein-gold nanoparticle assembly. J. Inorg. Biochem 130, 59–68. [PubMed: 24176920]
16. Zhang L, Swift J, Butts CA, Yerubandi V, and Dmochowski IJ (2007) Structure and activity of apoferritin-stabilized gold nanoparticles. J. Inorg. Biochem 101, 1719–1729. [PubMed: 17723241]
17. Zou W, et al. (2016) Expression, purification, and characterization of recombinant human L-chain ferritin. Protein Expression Purif 119, 63–68.
18. Guo J, et al. (2017) Efficient expression of recombinant human heavy chain ferritin (FTH1) with modified peptides. Protein Expression Purif. 131, 101–108.
19. Seo H-Y, and Kim K-S (2011) Purification and biochemical characterization of recombinant human H-ferritins from Saccharomyces cerevisiae. Biotechnol. Bioprocess Eng. 16, 360–365.
20. Truffi M, et al. (2016) Ferritin nanocages: A biological platform for drug delivery, imaging and theranostics in cancer. Pharmacol. Res 107, 57–65. [PubMed: 26968122]
21. Li JY, et al. (2009) Scara5 is a Ferritin Receptor Mediating Non-Transferrin Iron Delivery. Dev. Cell 16, 35–46. [PubMed: 19154717]
22. Khoshnejad M, et al. (2016) Vascular Accessibility of Endothelial Targeted Ferritin Nanoparticles. Bioconjugate Chem 27, 628–637.

23. Dehal PK, et al. (2010) Magnetizable antibody-like proteins. Biotechnol. J 5, 596–604. [PubMed: 20518063]
24. Lin X, et al. (2011) Chimeric ferritin nanocages for multiple function loading and multimodal imaging. Nano Lett 11, 814–819. [PubMed: 21210706]
25. van Vught R, Pieters RJ, and Breukink E (2014) Site-Specific Functionalization of Proteins and Their Applications To Therapeutic Antibodies. Comput. Struct. Biotechnol. J 9, e201402001. [PubMed: 24757499]
26. Schumacher D, Hackenberger CPR, Leonhardt H, and Helma J (2016) Current Status: Site-Specific Antibody Drug Conjugates. J. Clin. Immunol. 36, 100–107. [PubMed: 27003914]
27. Dennler P, Fischer E, and Schibli R (2015) Antibody Conjugates: From Heterogeneous Populations to Defined Reagents. Antibodies 4, 197–224.
28. Axup JY, et al. (2012) Synthesis of site-specific antibody-drug conjugates using unnatural amino acids. Proc. Natl. Acad. Sci. U. S. A 109, 16101–6. [PubMed: 22988081]
29. Hallam TJ, Wold E, Wahl A, and Smider VV (2015) Antibody conjugates with unnatural amino acids. Mol. Pharmaceutics 12, 1848–1862.
30. Soundrarajan N (2012) Conjugation of Proteins by Installing BIO-Orthogonally Reactive Groups at Their N-Termini. PLoS One 7, e46741. [PubMed: 23056430]
31. Wang K, et al. (2014) Optimized orthogonal translation of unnatural amino acids enables spontaneous protein double-labelling and FRET. Nat. Chem 6, 393–403. [PubMed: 24755590]
32. Lang K, and Chin JW (2014) Cellular Incorporation of Unnatural Amino Acids and Bioothogonal Labeling of Proteins. Chem. Rev. 114, 4764–4806. [PubMed: 24655057]
33. Santoro SW (2003) An archaebacteria-derived glutamyl-tRNA synthetase and tRNA pair for unnatural amino acid mutagenesis of proteins in Escherichia coli. Nucleic Acids Res. 31, 6700–6709. [PubMed: 14627803]
34. Zimmerman ES, et al. (2014) Production of Site-Specific Antibody – Drug Conjugates Using Optimized Non-Natural Amino Acids in a Cell-Free Expression System. Bioconjugate Chem. 25, 351–361.
35. Patel KG, and Swartz JR (2011) Surface functionalization of virus-like particles by direct conjugation using azide-alkyne click chemistry. Bioconjugate Chem. 22, 376–387.
36. Fraczkiewicz R, and Braun W (1998) Exact and efficient analytical calculation of the accessible surface areas and their gradients for macromolecules. J. Comput. Chem. 19, 319–333.
37. Wang Z, et al. (2006) Structure of human ferritin L chain. Acta Crystallogr., Sect. D: Biol. Crystallogr 62, 800–806. [PubMed: 16790936]
38. MaHam A, Tang Z, Wu H, Wang J, and Lin Y (2009) Protein-based nanomedicine platforms for drug delivery. Small 5, 1706–1721. [PubMed: 19572330]
39. Frandsen JL, and Ghandehari H (2012) Recombinant protein-based polymers for advanced drug delivery. Chem. Soc. Rev 41, 2696. [PubMed: 22344293]
40. Kaczmarczyk SJ, Sitaraman K, Young HA, Hughes SH, and Chatterjee DK (2011) Protein delivery using engineered virus-like particles. Proc. Natl. Acad. Sci. U. S. A 108, 16998–17003. [PubMed: 21949376]
41. Anumolu R, et al. (2011) Fabrication of highly uniform nanoparticles from recombinant silk-elastin-like protein polymers for therapeutic agent delivery. ACS Nano 5, 5374–5382. [PubMed: 21696150]
42. Khaled G, Frandsen J, Scharff S, Gustafson J, Cappello J, Li D, O'Malley BW Jr., and Ghandehari H (2010) Silk-elastinlike protein polymers improve the efficacy of adenovirus thymidine kinase enzyme prodrug therapy of head and neck tumors Khaled. J. Gene Med. 12, 572–579. [PubMed: 20603862]
43. Park WM, and Champion JA (2014) Thermally triggered self-assembly of folded proteins into vesicles. J. Am. Chem. Soc 136, 17906–17909. [PubMed: 25495148]
44. Kullberg M, Mann K, and Anchordoquy TJ (2012) Targeting Her-2+ breast cancer cells with bleomycin immunoliposomes linked to LLO. Mol. Pharmaceutics 9, 2000–2008.
45. Kullberg M, McCarthy R, and Anchordoquy TJ (2013) Systemic tumor-specific gene delivery. J. Controlled Release 172, 730–736.

46. Gunawan RC, Almeda D, and Auguste DT (2011) Complementary targeting of liposomes to IL-1a and TNF-a activated endothelial cells via the transient expression of VCAM1 and E-selectin. Biomaterials 32, 9848–9853. [PubMed: 21944721]
47. Rafat M, Rotenstein LS, You JO, and Auguste DT (2012) Dual functionalized PVA hydrogels that adhere endothelial cells synergistically. Biomaterials 33, 3880–3886. [PubMed: 22364701]
48. Zan X, Garapaty A, and Champion JA (2015) Engineering Polyelectrolyte Capsules with Independently Controlled Size and Shape. Langmuir 31, 7601–7608. [PubMed: 26114616]
49. Beavers KR, et al. (2016) Porous Silicon and Polymer Nanocomposites for Delivery of Peptide Nucleic Acids as Anti-MicroRNA Therapies. Adv. Mater 28, 7984–7992. [PubMed: 27383910]
50. Werfel TA, Swain C, Nelson CE, Kilchrist KV, Evans BC, and Martina Miteva CLD (2016) Hydrolytic charge-reversal of PEGylated polyplexes enhances intracellular un-packaging and activity of siRNA. J. Biomed. Mater. Res., Part A 28, 1304–1314.
51. Zhang J, Cui J, Deng Y, Jiang Z, and Saltzman WM (2016) Multifunctional Poly(amine-co-ester-co-ortho ester) for Efficient and Safe Gene Delivery. ACS Biomater. Sci. Eng. 2, 2080–2089. [PubMed: 28649641]
52. Gupta A, Bahal R, Gupta M, Glazer PM, and Saltzman WM (2016) Nanotechnology for delivery of peptide nucleic acids (PNAs). J. Controlled Release 240, 302–311.
53. Thorek DLJ, Chen AK, Czupryna J, and Tsourkas A (2006) Superparamagnetic iron oxide nanoparticle probes for molecular imaging. Ann. Biomed. Eng. 34, 23–38. [PubMed: 16496086]
54. Lakshmanan S, et al. (2014) Physical energy for drug delivery; poration, concentration and activation. Adv. Drug Delivery Rev. 71, 98–114.
55. Young JL, and Dean DA (2015) Electroporation-Mediated Gene Delivery, Advances in Genetics Vol 89, Elsevier Ltd.
56. Lin X, Barravecchia M, Kothari P, Young JL, and Dean DA (2016) β1-Na+,K+-ATPase gene therapy upregulates tight junctions to rescue lipopolysaccharide-induced acute lung injury. Gene Ther. 23, 489–499. [PubMed: 26910760]
57. Jang S, Sachin K, Lee H, Kim DW, and Lee HS (2012) Development of a simple method for protein conjugation by copper-free click reaction and its application to antibody-free Western blot analysis. Bioconjugate Chem. 23, 2256–61.
58. Wals K, and Ovaa H (2014) Unnatural amino acid incorporation in E. coli: current and future applications in the design of therapeutic proteins. Front. Chem. 2, 15. [PubMed: 24790983]
59. Sakamoto K (2002) Site-specific incorporation of an unnatural amino acid into proteins in mammalian cells. Nucleic Acids Res. 30, 4692–4699. [PubMed: 12409460]
60. Liu W, Brock A, Chen S, Chen S, and Schultz PG (2007) Genetic incorporation of unnatural amino acids into proteins in mammalian cells. Nat. Methods 4, 239–244. [PubMed: 17322890]
61. Huang CJ, Lin H, and Yang X (2012) Industrial production of recombinant therapeutics in Escherichia coli and its recent advancements. J. Ind. Microbiol. Biotechnol. 39, 383–399. [PubMed: 22252444]
62. Sanchez-Garcia L, et al. (2016) Recombinant pharmaceuticals from microbial cells: a 2015 update. Microb. Cell Fact. 15, 33. [PubMed: 26861699]
63. Zern BJ, et al. (2013) Reduction of nanoparticle avidity enhances the selectivity of vascular targeting and PET detection of pulmonary inflammation. ACS Nano 7, 2461–2469. [PubMed: 23383962]
64. Simone EA, et al. (2012) Endothelial targeting of polymeric nanoparticles stably labeled with the PET imaging radioisotope iodine-124. Biomaterials 33, 5406–5413. [PubMed: 22560201]
65. Rossin R, Muro S, Welch MJ, Muzykantov VR, and Schuster DP (2007) In vivo Imaging of 64Cu-Labeled Polymer Nanoparticles Targeted to the Lung Endothelium. J. Nucl. Med. 49, 103–111. [PubMed: 18077519]
66. Greineder CF (2013) Vascular immunotargeting to endothelial determinant ICAM-1 enables optimal partnering of recombinant scFv-Thrombomodulin fusion with endogenous cofactor. PLoS One 8, e80110. [PubMed: 24244621]
67. Atochina EN, Balyasnikova IV, Danilov SM, Granger DN, Fisher AB, and Muzykantov VR (1998) Immunotargeting of catalase to ACE or ICAM-1 protects perfused rat lungs against oxidative stress. Am. J. Physiol. 275, L806–17. [PubMed: 9755114]

68. Murciano JC, et al. (2003) ICAM-directed vascular immunotargeting of antithrombotic agents to the endothelial luminal surface. Blood 101, 3977–3984. [PubMed: 12531816]

69. Muro S, et al. (2003) Slow intracellular trafficking of catalase nanoparticles targeted to ICAM-1 protects endothelial cells from oxidative stress. AJP Cell Physiol. 285, C1339–C1347.

70. Luzzago A, and Cesareni G (1989) Isolation of point mutations that affect the folding of the H chain of human ferritin in E.coli. EMBO J. 8, 569–76. [PubMed: 2656256]

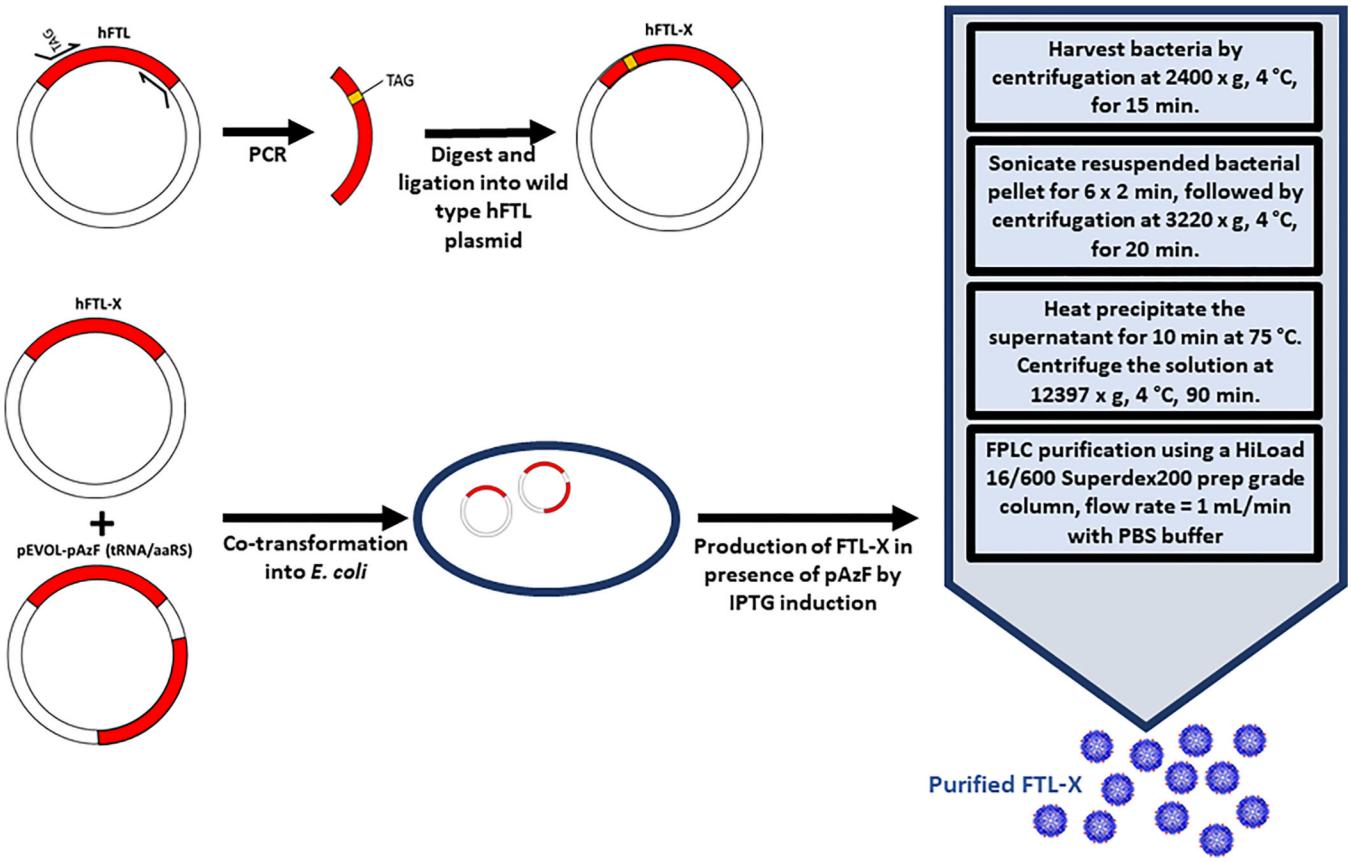

Figure 1.

Illustration of FTL-X variant construction and production in *E. coli*. Human FTL was modified by PCR cloning method to incorporate amber stop codon (TAG) at desired position in the FTL cDNA. The FTL-X plasmid was cotransformed along with the pEVOL-AzF vector, which encodes the tRNA/aaRS pair for para-azido-L-phenylalanine (pAzF),[33] into competent *E. coli*. Large scale production was performed by IPTG induction in the presence of pAzF. FTL-X was extracted by sonication and heat precipitation followed by purification by FPLC.

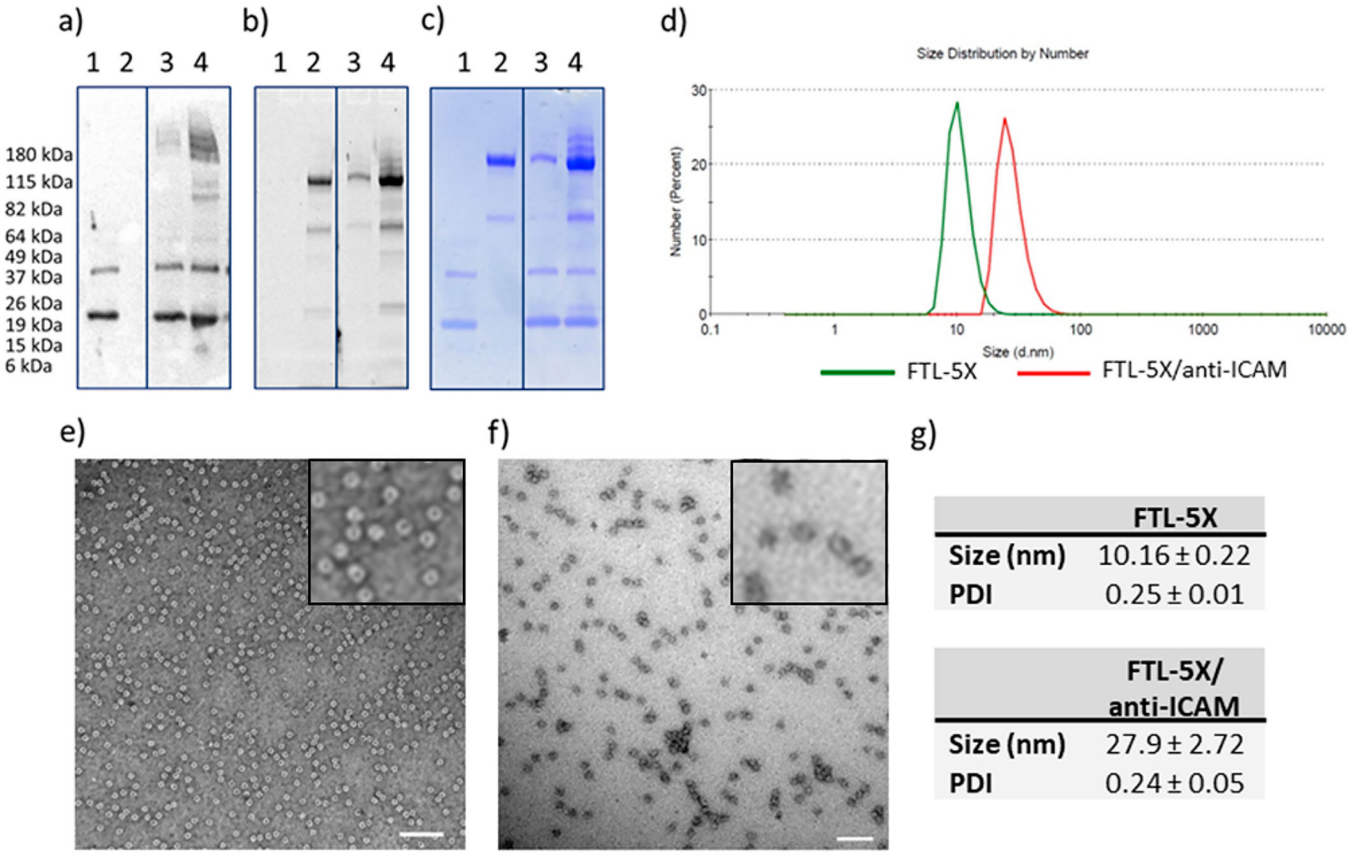

	FTL-5X
Size (nm)	10.16 ± 0.22
PDI	0.25 ± 0.01

	FTL-5X/ anti-ICAM
Size (nm)	27.9 ± 2.72
PDI	0.24 ± 0.05

Figure 2.

Characterization of FTL-5X and FTL-5X/anti-ICAM conjugates. (a) Western blot (staining for hFTL), (b) fluorescence scan, and (c) SDS-PAGE analysis of FTL-5X conjugated to AlexaFluor488 labeled anti-ICAM at different molar ratios. Lane numbers indicate the following: (1) FTL-5X, (2) anti-ICAM, (3) FTL-5X/anti-ICAM at molar ratio of 1 to 2, and (4) FTL-5X/anti-ICAM at molar ratio of 1 to 10. TEM images and size analysis of FTL-5X and antibody conjugates. TEM images of (e) FTL-5X and (f) FTL-5X/anti-ICAM. Scale bar: 100 nm. Particle size analysis (size distribution by number) obtained by DLS for (d) FTL-5X, and FTL-5X/anti-ICAM, as well as their (g) mean size and polydispersity index (PDI).

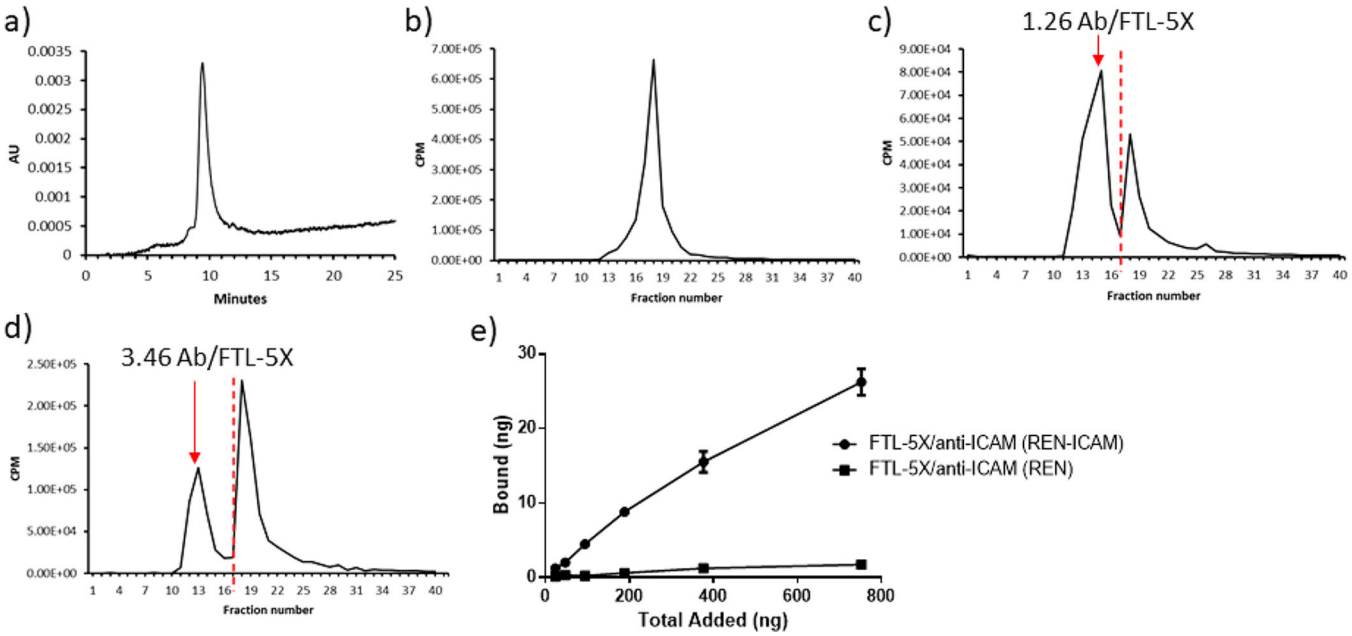

Figure 3.

Quantitative analysis of number of radiolabeled whole antibody conjugated to FTL-5X using HPLC. Antibody was radiolabeled with ^{125}I, followed by conjugation to FTL-5X at different molar ratios. HPLC absorbance trace of (a) FTL-5X, and radiotraces of (b) anti-ICAM, (c) FTL-5X/ anti-ICAM (1 to 2 molar ratio), (d) FTL-5X/anti-ICAM (1 to 10 molar ratio). Red colored dashed line indicates the cutoff line used for calculation of areas under the curve (AUC) for conjugate vs free antibody peaks. (e) *In vitro* binding of ^{125}I-labeled targeted FTL-5X to ICAM positive and negative REN cells. FTL-5X was ^{125}I-labeled prior to antibody conjugation. Cells were grown to confluence and incubated with targeted FTL-5X nanocarriers for 1 h at 37 °C. Bound radiolabeled targeted nanocages were measured by gamma counter.

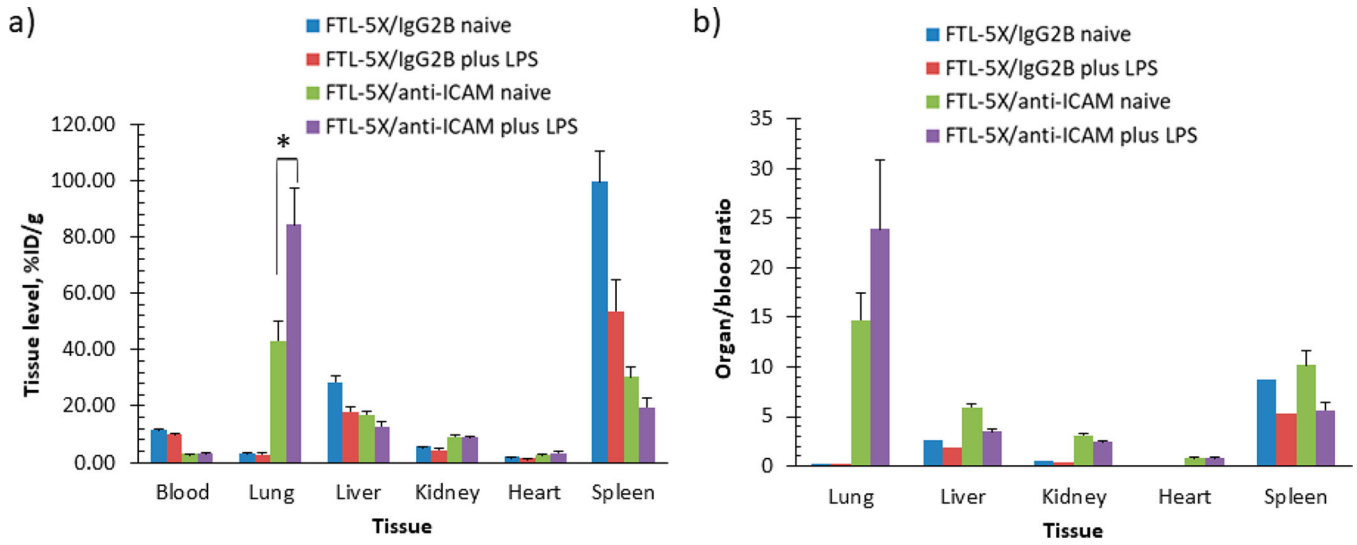

Figure 4.

In vivo targeting of ^{125}I-labeled targeted FTL-5X to ICAM-1. (a) Biodistribution of ^{125}I-labeled FTL-5X conjugated to anti-ICAM and IgG2b isotype control in naïve and LPS-treated mice at 30 min. Tissue uptake is indicated as mean ± SEM ($n = 3$). (b) Localization ratio of selected organs. Significant differences determined by t test with Bonferroni correction to account for multiple comparisons (*$p < 0.05$).

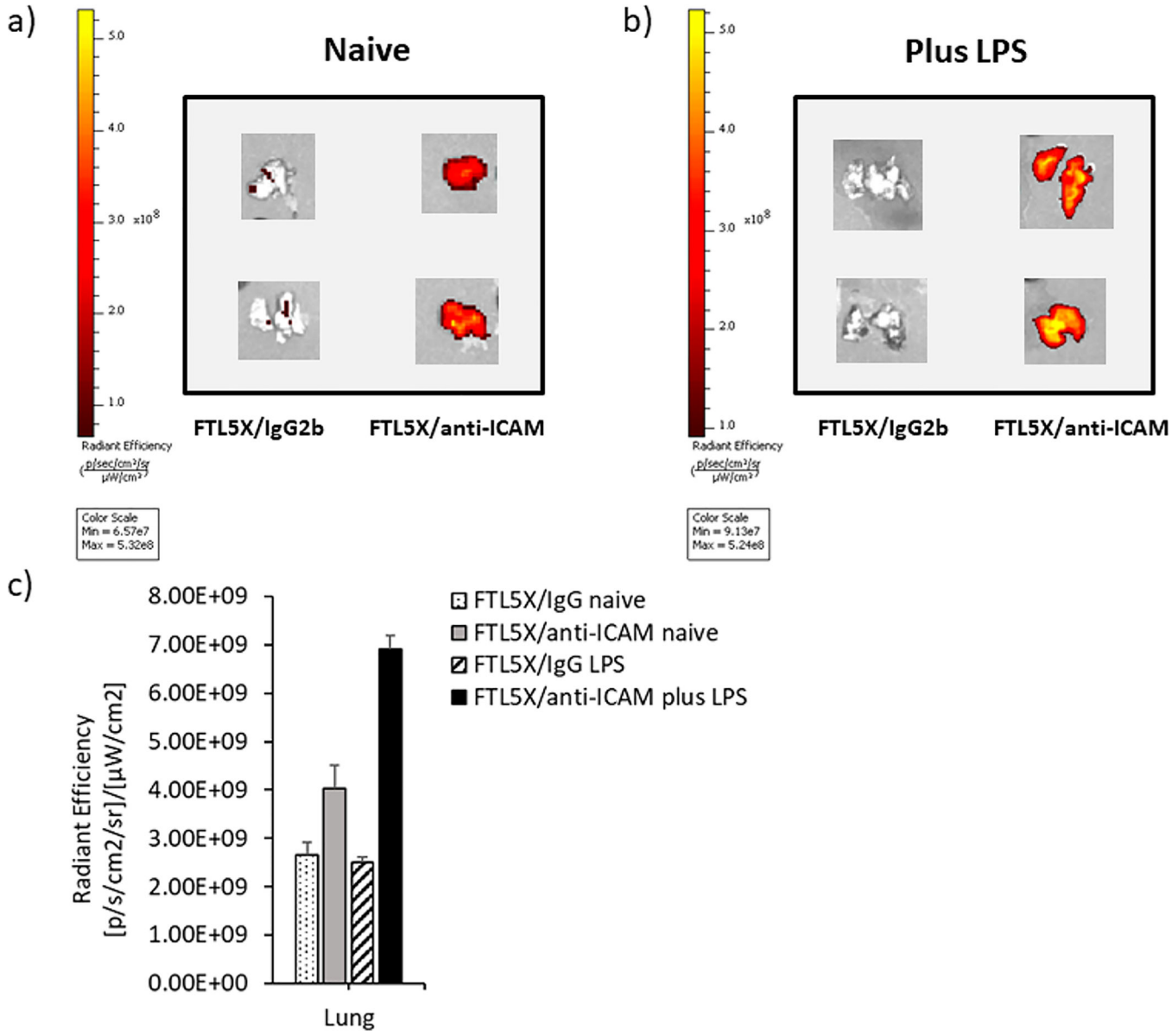

Figure 5.

Near-infrared imaging of lungs harvested from mice treated with targeted FTL-5X. *Ex vivo* imaging of lungs treated with AF750-labeled FTL-5X conjugated to anti-ICAM and IgG2b isotype control in (a) naive and (b) LPS-treated mice at 30 min. (c) Fluorescence intensity quantification of lungs.